ARCHIVES OF ELECTRICAL ENGINEERING VOL. 74(1), pp. 269–289 (2025)

DOI 10.24425/aee.2025.153024

A neural-enhanced active disturbance load-side speed control of an electric drive with a flexible link

GRZEGORZ KACZMARCZYK [1], RADOSLAW STANISLAWSKI [1], MARCIN KAMINSKI [1]✉, KACPER KASPRZAK [2], DANTON DIEGO FERREIRA [3]

[1] *Wroclaw University of Science and Technology*
Poland

[2] *Poznan University of Technology*
Poland

[3] *Federal University of Lavras*
Brazil

e-mail: ✉ *marcin.kaminski@pwr.edu.pl*

(Received: 03.10.2024, revised: 10.02.2025)

Abstract: The paper is focused on improvements of the conventional speed controller based on Active Disturbance Rejection Control (ADRC) applied for a two-mass electric drive system. The described ADRC structure is based on load-side speed measurement. The paper compares conventional structure dynamics with overall system behavior in the case plant parameters are changed. The proposed ADRC algorithm extension performs soft controller parameters adjustment to improve the dynamics and plant response. The presented approach accomplishes adaptation capabilities with the use of a Radial Basis Function Neural Network (RBFNN). The article presents the dynamic response of the plant controlled by the conventional ADRC algorithm and the designed neural adaptation extension. The results are based on the performed experimental tests.

Key words: active disturbance rejection control, adaptive control, electric drives, neural network, two-mass system

1. Introduction

Modern electric drive systems are designed to provide a highly dynamic plant response. Moreover, the demand is that the effect of parameter uncertainty and external disturbances must be minimal. Assuming an ideally stiff connection between the motor and the load machine is usually

sufficient. However, in certain applications, such as robotic structures [1, 2], wind turbines [3], and electric vehicles [4], the flexibility of the connecting element must be taken into account. Current trend in robotic structure design revolves around manufacturing the elements from lighter materials for lower energy consumption and increased operation safety. In turn, the decrease in weight resulting from the change in materials used causes another point of elasticity. From the control system perspective, finite stiffness of the mechanical structure is an undesirable feature. The oscillations of state variables, which are the direct effect of the elastic construction, cause problems with control precision, machine longevity, and stability [5]. The oscillations must therefore be mitigated. Even though installing mechanical dampeners might appear as an adequate solution, they require further complication of the mechanical structure, increase the overall cost of the drive system, and enforce more frequent maintenance. Therefore, an algorithmic approach to oscillation damping is investigated.

Multiple different techniques are used in the literature to control two-mass systems. One of the most commonly selected algorithms is PID control [6]. It is appealing because of its low complexity and ease of implementation on programmable devices. However, due to limited information obtained from the control structure, PID control seldom provides satisfactory results. Improvements can be obtained through additional feedback [7]. Also, with the supplementary signals, the form of the controller can be changed to State Feedback Control [8, 9]. Attempts are also made to change the description of the plant through the combination of Partial and Ordinary Differential Equations to obtain wave models [10]. All the approaches, despite providing high control quality, have one common weakness: their vulnerability to plant parameter changes. Tuning of those controllers requires the plant parameters to be fully known. Even if the plant is meticulously identified, its parameters can undergo changes during its operation. Therefore, robustness becomes a highly sought-after feature of speed controllers in multi-mass systems.

Robust control algorithms ensure proper operation of the plant within a predefined range of its possible parameter changes. The controller gains and structure remain unaltered at all times. Examples of such strategies include H∞ Control [11], Fuzzy Logic Control [12], Sliding Mode Control [13], and Active Disturbance Rejection Control (ADRC) [14–17]. Especially the last approach has lately become very popular in research institutes around the world. ADRC does not require the exact plant model to be known beforehand. In this method, it is implemented as a multi-integrator block. The principle of this strategy is to treat all the internal and external disturbances as an additional variable supplied to the control structure. The algorithm consists of three main blocks: a state observer, a controller, and a rejector. Information about the state of the plant and its disturbances is obtained from the state observer. The state variables are later fed back to the error-based controller block, while the disturbance is sent to the rejector to establish the final control signal.

ADRC performs according to expectations when the parameters of the plant remain within the anticipated range. If the changes exceed that range, significant deterioration of the system response could happen. Greater changes in plant parameters would have to be mitigated through gain adaptation [18]. One of the most investigated methods of incorporating adaptive properties in the control structure is to combine the algorithm with a neural network. Often Radial Basis Function Neural Networks (RBFNNs) are selected [19, 20]. In such a network each radial neuron represents a cluster of the data space, and their weighted superposition is the output of the neural network. They are an excellent tool for establishing a relationship between the input and the output

data, especially if the relationship is highly nonlinear. Adaptive properties are achieved if the training of the RBFNN is performed simultaneously with the operation of the plant. The weights of the network are then adequately adjusted to provide the needed signal.

The main contribution and goal of this study is to provide a control structure for electric drives with an elastic connection capable of withstanding plant parameter changes and external disturbances. A two-mass system is selected as the plant. The proposed algorithm provides robustness of ADRC strategy combined with adaptive properties of an RBFNN. The paper is organized as follows. First, the mathematical model of the plant and preliminary information regarding ADRC are presented. Then, the proposed neural-enhanced ADRC structure is introduced. Its performance is tested in numerical studies, and then verified on a laboratory test bench. The obtained results are summarized and discussed in the final part of the article.

2. Plant model

The object analyzed in the article is an electric drive with a long, elastic shaft connecting the motor with the load. Comprehensive analysis of the considered drive is presented in chapter 5 of this article. Such a construction can be modeled as a two-mass system. The mechanical part can be described with the following set of equations:

$$\begin{cases} J_1\dot{\omega}_1 = T_e - (T_T + D(\omega_1 - \omega_2)) - T_{f1} \\ J_2\dot{\omega}_2 = (T_T + D(\omega_1 - \omega_2)) - T_L - T_{f2} \end{cases} \tag{1}$$

and

$$\begin{aligned} T_T &= K_C(\alpha_1 - \alpha_2) \\ \dot{T}_T &= K_C(\omega_1 - \omega_2) \end{aligned}, \tag{2}$$

where: ω_1, ω_2 are the rotational speeds of the motor and the load, respectively, T_e is the electromagnetic torque, T_T is the torsional torque, $\dot{T}_T$ is the torsional torque time derivative, D is the damping coefficient, T_L is the torque load, K_C is the stiffness coefficient, T_{f1}, T_{f2} are the friction torques, $\alpha_1\alpha_2$ are the shaft angular displacements near the motor and the load, respectively.

To analyze the most critical mode of operation, during further analysis the damping coefficient D is assumed to be 0. The graphical representation of the equations is shown in Fig. 1. In this model, the electromagnetic torque T_e acts as an input signal, and angular speed of the load is regarded as the plant output.

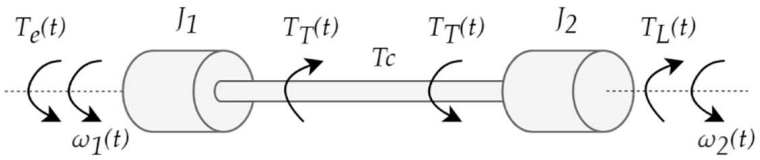

Fig. 1. The graphical representation of the two-mass system model

A strong relationship between the state variables can be observed. This dependence causes the oscillations to appear in the system response. A control structure for such a system has to fulfill multiple criteria. The strategy must be capable of mitigating the oscillations that appear in the plant response. Moreover, robustness against parameter uncertainty must be provided. Finally, the ability to withstand external disturbances must also be guaranteed. In this study, ADRC control strategy is selected and enhanced with adaptive properties from an RBFNN.

3. The proposed control strategy equipped with active ADRC controller neural adjuster

Nowadays, due to strict demands forced by industry, efficient control strategies are developed. One of the most common control methods featuring robust properties is known as Active Disturbance Rejection Control. Its main assumption is that the exact mathematical form of the plant does not need to be known, as it can be described in the form of a multi-integrator block. Moreover, one of the most essential principles of the ADRC strategy assumes that both the external and internal disruptions (e.g. load torque, changed friction value, stiffness, or elasticity) are treated as an additional, combined disturbance affecting the system. The precise form of the disturbance can also be omitted, which constitutes a huge advantage of the ADRC over similar structures. The proposed algorithm concerns the Active Disturbance Rejection Control variant, which strongly refers to the two-mass electric drive system issue. The described approach was first developed and briefly described in the series of scientific papers [21, 22]. The algorithm described in those manuscripts features the lack of necessity of using a Tracking Differentiator block. It is also based on the idea of load side speed measurement only. That being said, the proposed structure facilitates the implementation process and increases the durability of the drive by minimizing the number of mechanical sensors used. Therefore, the aspects of the described ADRC approach constitute an undeniable prevalence of the Load Side Speed Measurement ADRC controller over similar, two-mass system control algorithms.

The Active Disturbance Rejection Control algorithm consists of three primary elements: the main controller, the rejector, and the Extended State Observer. The role of the controller is to produce an initial form of the control signal. Then, after executing proper calculations, the estimated disturbance is subtracted from the control signal in the Rejector block. Having conducted the mentioned subtraction, the final form of the control signal is relayed to the further part of the control loop. The Extended State Observer is considered the most critical element of the whole ADRC strategy. Not only is it responsible for calculating consecutive state space variables (e.g. derivatives of speed), but it is also in charge of estimating the additional, extended state variable, where the combined disturbance value is stored. The Extended State Observer is based on the Luenberger model, which gives the possibility to shape its internal dynamics. The main role of the state observer is to recreate the internal plant dynamics without the necessity of using its mathematical equation. Therefore, the state space variables are also estimated on-line, which has a positive impact on the control system quality, as the measurement noise is not needlessly amplified during derivative calculations.

In order to simplify the plant model to the form of a multi-integrator block, the internal dynamics of the plant need to be treated as an additional disturbance as well. That being said, a simplified plant can be presented with the scheme shown in Fig. 2.

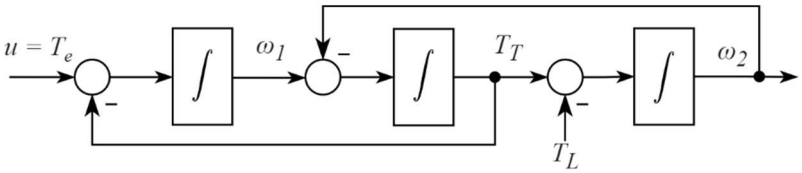

Fig. 2. The plant model presented in the form of a multi-integrator block

Considering the fact that the load side speed feedback is available only, and taking the simplified plant model into account, a third load side speed derivative needs to be calculated in order to obtain a desired motor speed change. That being said, referring to the plant model, shown in Fig. 2, the abovementioned consideration can be described with the following formula:

$$\frac{\partial \omega_1(t)}{\partial t} = \frac{\partial^3 \omega_2(t)}{\partial t^3}. \tag{3}$$

Calculating the third derivative of $\dot{\omega}_2$ leads to the equations:

$$J_2\dddot{\omega}_2 = \left(\ddot{T}_T + D\left(\ddot{\omega}_1 - \ddot{\omega}_2\right)\right) - \ddot{T}_L - \ddot{T}_{f2} = \left(K_C\left(\dot{\omega}_1 - \dot{\omega}_2\right) + D\left(\ddot{\omega}_1 - \ddot{\omega}_2\right)\right) - \ddot{T}_L - \ddot{T}_{f2}, \tag{4}$$

$$\dddot{\omega}_2 = \frac{K_C}{J_2}\left(\ddot{\omega}_1 - \ddot{\omega}_2\right) + \frac{D}{J_2}\left(\ddot{\omega}_1 - \dddot{\omega}_2\right) - \frac{1}{J_2}\dddot{T}_L - \frac{1}{J_2}\dddot{T}_{f2}. \tag{5}$$

The first ω_1 derivative can be described as:

$$\dot{\omega}_1 = \frac{1}{J_1}T_e - \frac{1}{J_1}T_T - \frac{D}{J_1}\left(\omega_1 - \omega_2\right) - \frac{1}{J_1}T_{f1}. \tag{6}$$

Substituting $\dot{\omega}_1$ with Eq. (6) leads to:

$$\ddot{\omega}_2 = \frac{K_C}{J_2}\left(\frac{1}{J_1}T_e - \frac{1}{J_1}T_T - \frac{D}{J_1}\left(\omega_1 - \omega_2\right) - \dot{\omega}_2 - \frac{1}{J_1}T_{f1}\right) + \frac{D}{J_2}\left(\ddot{\omega}_1 - \ddot{\omega}_2\right) - \frac{1}{J_2}\ddot{T}_L - \frac{1}{J_2}\ddot{T}_{f2}, \tag{7}$$

$$\begin{aligned}\ddot{\omega}_2 = {} & \frac{K_C}{J_2J_1}T_e - \frac{K_C}{J_2J_1}\left(K_C\left(\alpha_1 - \alpha_2\right) + D\left(\omega_1 - \omega_2\right)\right) - \frac{K_C}{J_2}\dot{\omega}_2 - \frac{K_C}{J_2J_1}T_{f1} \\ & + \frac{D}{J_2}\left(\ddot{\omega}_1 - \ddot{\omega}_2\right) - \frac{1}{J_2}\ddot{T}_L - \frac{1}{J_2}\ddot{T}_{f2},\end{aligned} \tag{8}$$

$$\begin{aligned}\ddot{\omega}_2 = {} & \frac{K_C}{J_2J_1}T_e - \frac{K_C}{J_2J_1}\left(K_C\left(\alpha_1 - \alpha_2\right) + D\omega_1\right) + \frac{K_CD}{J_2J_1}\omega_2 - \frac{K_C}{J_2}\dot{\omega}_2 - \frac{K_C}{J_2J_1}T_{f1} \\ & + \frac{D}{J_2}\ddot{\omega}_1 - \frac{D}{J_2}\ddot{\omega}_2 - \frac{1}{J_2}\ddot{T}_L - \frac{1}{J_2}\ddot{T}_{f2}.\end{aligned} \tag{9}$$

Assuming that

$$b = \frac{K_C}{J_2J_1},$$

$$u = T_e,$$

$$A = -\frac{K_C}{J_2 J_1}\left(K_C\left(\alpha_1 - \alpha_2\right) + D\omega_1\right) - \frac{K_C}{J_2 J_1}T_{f1} + \frac{D}{J_2}\ddot{\omega}_1 - \frac{1}{J_2}\ddot{T}_{L} - \frac{1}{J_2}\ddot{T}_{f2},$$

the above expression can be simplified to the following form:

$$\ddot{\omega}_2 = -\frac{D}{J_2}\ddot{\omega}_2 - \frac{K_C}{J_2}\dot{\omega}_2 + bD\omega_2 + bu + A. \tag{10}$$

Then, the phase plane variables can be assumed as:

$$\begin{cases} x_1 = \omega_2 \\ x_2 = \dot{\omega}_2 \\ x_3 = \ddot{\omega}_2 \end{cases}. \tag{11}$$

So, the state space equation of the two-mass drive system can be presented as:

$$\begin{cases} \dot{x}_1 = \dot{\omega}_2 \\ \dot{x}_2 = \ddot{\omega}_2 \\ \dot{x}_3 = \dddot{\omega}_2 \\ y = x_1 \end{cases} = \begin{cases} \dot{x}_1 = \dot{\omega}_2 \\ \dot{x}_2 = \ddot{\omega}_2 \\ \dot{x}_3 = -\dfrac{D}{J_2}\ddot{\omega}_2 - \dfrac{K_c}{J_2}\dot{\omega}_2 + bu + A \\ y = x_1 \end{cases}. \tag{12}$$

However, considering the fact that the Extended State Observer architecture includes the additional state space variable incorporating the information about the combined disturbance, the extended variable can be defined as:

$$x_4 = f\left(t, \omega_2, \dot{\omega}_2, \ddot{\omega}_2\right). \tag{13}$$

Thus, the final state space equation of the examined two-mass electric drive unit can be expressed as follows:

$$\begin{cases} \dot{x}_1 = \dot{\omega}_2 \\ \dot{x}_2 = \ddot{\omega}_2 \\ \dot{x}_3 = x_4 + bu \\ \dot{x}_4 = \dot{f}\left(t, \omega_2, \dot{\omega}_2, \ddot{\omega}_2\right) \\ y = x_1 \end{cases}, \tag{14}$$

where:

$$\begin{aligned} f\left(t, \omega_2, \dot{\omega}_2, \ddot{\omega}_2\right) = & -\frac{D}{J_2}\ddot{\omega}_2 - \frac{K_C}{J_2}\dot{\omega}_2 + \frac{K_C}{J_2 J_1}D\omega_2 - \frac{K_C}{J_2 J_1}\left(K_C\left(\alpha_1 - \alpha_2\right) + D\omega_1\right) \\ & - \frac{K_C}{J_2 J_1}T_{f1} + \frac{D}{J_2}\ddot{\omega}_1 - \frac{1}{J_2}\ddot{T}_{L} - \frac{1}{J_2}\ddot{T}_{f2} \end{aligned} \tag{15}$$

is the combined disturbance equation.

Therefore, the precise form of the mathematical disturbance description is rejected, as it is estimated with the use of the estimation error (e_0). The final Extended State Observer equation

can be described with the following expression:

$$\begin{cases} e_0 = z_1 + y \\ \dot{z}_1 = z_2 + B_1 e_0 \\ \dot{z}_2 = z_3 + B_2 e_0 \\ \dot{z}_3 = z_4 + B_4 e_0 + bu \\ \dot{z}_4 = B_4 e_0 \end{cases}, \tag{16}$$

where z_4 is the estimated disturbance value.

According to the approach, presented in [21], the controller equation can be defined as:

$$u_0 = k_p \left(\omega_{\text{ref}} - z_1\right) - k_d z_2 - k_{dd} z_3, \tag{17}$$

where k_p, k_d, k_{dd} are the controller gains. The final control signal u is established in the disturbance rejector block, and is calculated using the following formula:

$$u = \frac{u_0 - z_4}{b}. \tag{18}$$

Considering the fact that the derivative of the third state space variable can be also rewritten as:

$$\dot{x}_3 = \dddot{\omega}_2 = f\left(t, \omega_2, \dot{\omega}_2, \ddot{\omega}_2\right) + bu. \tag{19}$$

After combining Eqs. (18) and (19) the final form of the third derivative of the load speed can be simplified to:

$$\dot{x}_3 = \dddot{\omega}_2 = u_0. \tag{20}$$

The final controller gains are determined by the Pole Placement method. After switching the controller differential equation to the Laplace domain, the representative polynomial of the used controller can be obtained:

$$P(p) = p^3 + k_{dd} p^2 + k_d p - k_p, \tag{21}$$

where p is a Laplace operator. Considering the fact that the controller representative formula is a third order equation, a third order transfer polynomial needs to be assumed as a reference mathematical expression. The final reference equation can be described as follows:

$$M(p) = p^3 + 3\omega_r p^2 + 3\omega_r^2 p + \omega_r^3, \tag{22}$$

where ω_r is a controller cut-off frequency (design parameter). Having compared the $P(p)$ and $M(p)$ coefficients, a final set of controller gains can be presented as:

$$\begin{cases} k_p = \omega_r^3 \\ k_d = 3\omega_r^2 \\ k_{dd} = 3\omega_r \end{cases}. \tag{23}$$

Despite the fact that the ADRC algorithm is considered as a robust control technique, it turns out that its robustness can be increased. The b coefficient is the only factor in the ADRC control strategy, which is strictly related to the plant parameters. The controller gains values are based on the controller cut-off frequency. The standard solution provides robustness against changed

plant parameters. However, in that scenario, there are some inconveniences visible in the plant response which may affect the durability of the drive. The main goal of the proposed algorithm is to increase the accuracy of the way the actual load side speed follows its reference trajectory in terms of changed plant parameters. The main assumption of the proposed approach is to extend the standard ADRC algorithm with an additional, floating coefficient, which can adapt the values of the tuned parameters within limited range on the fly. The controller gains adjustment is related to the actual torque demand. By doing so, the controller gains are only increased in the dynamic states of the drive, when the torque demand is high. In the steady state of the drive gains are lowered not to force unnecessary vulnerability of the control system. The proposed solution significantly increases the overall plant response quality without the necessity of adjusting plant parameters (b coefficient). To achieve this, a Radial Basis Function Neural Network (RBFNN) has been employed. The overall scheme of the proposed control algorithm is shown in Fig. 3.

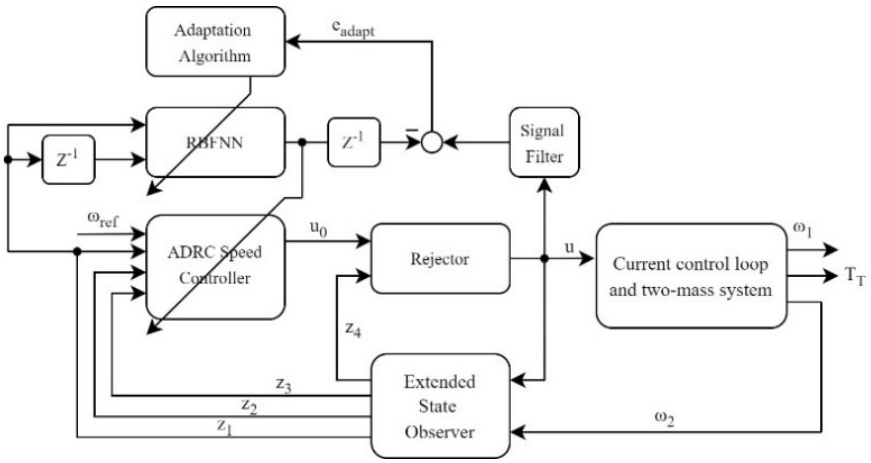

Fig. 3. The proposed ADRC structure with neural parameter adjustment

A Radial Basis Function Neural Network is a simple, feedforward neural network with one hidden layer of neurons. A typical RBFNN consists of three layers: input layer, hidden layer, and the output layer. Each neuron of the hidden layer is equipped with a Gaussian activation function. In the final part of the network there is a linear neuron which produces the final output of the neural structure. An RBFNN is trained on-line with the use of the gradient-descent method, which makes it a perfect tool for control loop applications. The simplicity and universality of the RBF network makes it a feasible tool in terms of demanding applications. It provides low resource utilization combined with adaptive capabilities. The structure of the applied RBFNN consists of 5 hidden neurons and is shown in Fig. 4.

The controller gains share strong interdependencies with the controller cut-off frequency. In order to keep the mentioned relationships unchanged, the floating coefficient modifies each controller gain proportionally. Thus, the final form of the controller output can be described as:

$$u_0 = \left(k_p \left(\omega_{\text{ref}} - z_1\right) - k_d z_2 - k_{dd} z_3\right) y_{\text{RBF}}, \tag{24}$$

where y_{RBF} is the RBFNN output, and can be defined as follows:

$$y_{\mathrm{RBF}} = \sum w_i h_i = \sum w_i \exp\left(-\frac{\|\boldsymbol{x}-\boldsymbol{C_i}\|^2}{2\sigma^2}\right), \tag{25}$$

where: $\boldsymbol{C}_i$ is the neuron center vector, $\boldsymbol{x}$ is the input, σ is the scaling factor, w_i is the weight coefficient, h_i is the activation function value.

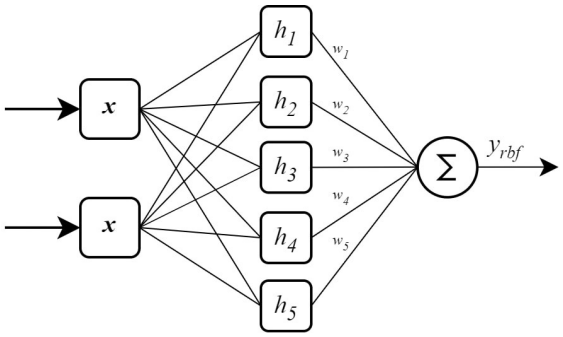

Fig. 4. The overall architecture of the applied neural network

The weight adaptation of the Radial Basis Function neural network is based on the gradient-descent method. Its main assumption is to inverse the data flow inside the network and calculate the derivatives of the cost function with respect to the weight coefficients. The value of the cost function needs to be minimized. For the sake of the proposed algorithm the cost function can be defined with the equation:

$$E(k) = \frac{1}{2}e^2(k), \tag{26}$$

where e is the adaptation algorithm error and can be described as:

$$e(k) = u_{\mathrm{ref}}(k) - y_{rbf}(k-1). \tag{27}$$

Following the gradient-descent method procedure, a cost function derivative needs to be calculated with respect to the weights:

$$\frac{\partial E(k)}{\partial w(k)} = \left(u_{\mathrm{ref}}(k) - y_{rbf}(k-1)\right)\left(\frac{\partial u_{\mathrm{ref}}(k)}{\partial w(k)} - \frac{\partial y_{rbf}(k-1)}{\partial w(k)}\right). \tag{28}$$

Considering the fact that the reference control signal value does not change in a specific time period it can be treated as a constant, which leads to the formula:

$$\frac{\partial u_{\mathrm{ref}}(k)}{\partial w(k)} = 0, \tag{29}$$

which simplifies Eq. (28) to the following form:

$$\frac{\partial E(k)}{\partial w(k)} = \left(u_{\mathrm{ref}}(k) - y_{rbf}(k-1)\right)\left(-\frac{\partial y_{rbf}(k-1)}{\partial w(k)}\right). \tag{30}$$

Considering Eq. (25), for the i-th weight coefficient, the above formula can be rewritten as:

$$\frac{\partial E(k)}{\partial w(k)} = \left(u_{\text{ref}}(k) - y_{rbf}(k-1)\right)\left(-\frac{\partial h_i(k-1)w_i(k-1)}{\partial w(k)}\right), \tag{31}$$

and after subsequent transformation:

$$\frac{\partial E(k)}{\partial w(k)} = \left(u_{\text{ref}}(k) - y_{rbf}(k-1)\right)\left(-\exp\left(-\frac{\|\boldsymbol{x}-\boldsymbol{C}_i\|^2}{2\sigma^2}\right)\right). \tag{32}$$

The update of network parameters is described as follows:

$$w(k+1) = w(k) - \eta\frac{\partial E(k)}{\partial w(k)} = w(k) + \eta\left(u_{\text{ref}}(k) - y_{rbf}(k-1)\right)\left(-\frac{\partial y_{rbf}(k-1)}{\partial w(k)}\right), \tag{33}$$

which can be simplified to the expression shown below:

$$w(k+1) = w(k) + \eta e(k)\, h(k-1). \tag{34}$$

The above considerations are confirmed after applying the chain rule:

$$\frac{\partial E(k)}{\partial w(k)} = \frac{\partial E(k)}{\partial e(k)}\frac{\partial e(k)}{\partial u(k-1)}\frac{\partial u(k-1)}{\partial w(k)} = -e(k)\, h(k-1), \tag{35}$$

where

$$\frac{\partial E(k)}{\partial e(k)} = e(k).$$

$$\frac{\partial e(k)}{\partial u(k-1)} = -1, \quad \text{because} \quad \frac{\partial e(k)}{\partial u(k-1)} = \frac{\partial u_{\text{ref}}(k) - \partial y_{\text{RBF}}(k-1)}{\partial u(k-1)} = \frac{\partial u_{\text{ref}}(k) - \partial u(k-1)}{\partial u(k-1)} = -1,$$

because $y_{\text{RBF}}(k-1) = u(k-1)$, which is a control signal.

$$\frac{\partial U(k)}{\partial w_i(k)} = h_i(k).$$

Stability analysis is a mandatory point of modern control systems design process. It is necessary to give a theoretical background concerning the information about the control system convergence. However, if neural networks are applied to the control loop, the stability issue becomes more sophisticated. Due to the high non-linearity of the control system equipped with neural models and the plant, typical analytical and graphical methods are not sufficient. In order to analyze the stability of the system, Lyapunov Theory needs to be employed. The Lyapunov Stability Theory is a groundbreaking tool, which allows one to examine the stability of the time-varying, dynamic systems with high non-linearity. Despite the fact that the ADRC stability has been proven in various publications (e.g. [22]), the use of the Neural Network has an enormous impact on the overall system stability and cannot be omitted.

The stability of the Radial Basis Function Neural Network is dependent on the adaptation algorithm convergence. Taking the basic Lyapunov Theory principle into account, a system is stable, when the following condition is ensured:

$$L = V\dot{V} \leq 0, \tag{36}$$

where V is the Lyapunov candidate function, and can be described as:

$$V = E(k) = \frac{1}{2}e^2(k). \tag{37}$$

When V is positive, it can be assumed that the system stays globally stable in the sense of Lyapunov, when the candidate function derivative is negative:

$$\dot{V} \leq 0. \tag{38}$$

Thus, the overall stability condition can be presented with the equation:

$$L = E(k)\dot{E}(k) \leq 0, \tag{39}$$

which means, that the following condition needs to be fulfilled:

$$\dot{E}(k) \leq 0. \tag{40}$$

Considering the fact that the weight coefficient in the following numerical step can be described with Eq. (33), a similar mathematical expression can be written with regard to the adaptation error [23]:

$$e(k+1) = e(k) + \Delta e(k), \tag{41}$$

and then, the following extension can be obtained [24]:

$$\Delta e(k) = \frac{\partial e(k)}{\partial w(k)} \cdot \Delta w(k). \tag{42}$$

Considering the fact that:

$$\Delta w(k) = -\eta \frac{\partial E(k)}{\partial w(k)} = -\eta e(k) \frac{\partial e(k)}{\partial w(k)}, \tag{43}$$

a following formula can be acquired:

$$\Delta e(k) = -\eta e(k) \frac{\partial e^2(k)}{\partial w^2(k)} \tag{44}$$

Thus, the combination of abovementioned mathematical considerations leads to the expression:

$$\dot{E}(k) = \Delta E(k) = \frac{1}{2}\left(e^2(k+1) - e^2(k)\right) = \frac{1}{2}\left[2e(k)\Delta e(k) + \Delta e^2(k)\right], \tag{45}$$

which after conducting a set of transformations can be rewritten as:

$$\dot{E}(k) = \frac{1}{2}\eta\left[\left(e(k)\frac{\partial e(k)}{\partial w(k)}\right)^2\left(\eta\frac{\partial e^2(k)}{\partial w^2(k)} - 2\right)\right]. \tag{46}$$

If the change in $E(k)$ is limited to be negative, this ensures that the Lyapunov function only decreases and proves that the system is stable. This is easily accomplished by ensuring the following equation:

$$\eta\frac{\partial e^2(k)}{\partial w^2(k)} - 2 < 0, \tag{47}$$

which can be written as:

$$0 < \eta < \frac{2}{\left(\frac{\partial e(k)}{\partial w(k)}\right)^2}, \tag{48}$$

where

$$\frac{\partial e(k)}{\partial w(k)} = \frac{\partial\left(\sqrt{2E(k)}\right)}{\partial w(k)} = \frac{1}{2\sqrt{2E(k)}}\frac{2\partial E(k)}{\partial w(k)} = \frac{1}{\sqrt{2E(k)}}\frac{\partial E(k)}{\partial w(k)}. \tag{49}$$

Substituting the expression $E(k)$ with Eq. (26), and simplifying the formula leads to:

$$0 < \eta < \frac{2}{\left(\frac{1}{e(k)}\frac{\partial E(k)}{\partial w(k)}\right)^2}, \tag{50}$$

which after proper substitution provides the final stability condition:

$$0 < \eta < \frac{2}{\left(\frac{1}{e(k)}\frac{\partial E(k)}{\partial w(k)}\right)^2}, \tag{51}$$

which can be rewritten as:

$$0 < \eta < \frac{2}{(-h(k-1))^2}. \tag{52}$$

4. Simulation tests

The examination of the proposed ADRC extension is divided into two main parts. The first one involves numerical testing. The whole simulation series is conducted in the MATLAB/Simulink environment. The first stage of the simulation tests contains the model preparation. The whole two-mass drive system is modeled with the use of triple-integrator architecture. It is accomplished by coupling three integrator blocks in series. Each of them is described with the transfer function in the Laplace domain. The consecutive mechanical time constants are presented below:

- $T_1 = 0.203$ s,
- $T_c = 0.0026$ s,
- $T_2 = 0.208$ s,

where: T_1 is the motor mechanical time constant, T_2 is the active load machine mechanical time constant, T_c is the mechanical time constant of the shaft.

The current control loop is modeled with the use of a 1-st order inertial block. It includes the current regulator, current measurement system, power converter, and electromagnetic circuit of the motor. The current control loop can be described with the following expression:

$$G_e(p) = \frac{1}{T_e(p) + 1}, \tag{53}$$

where $T_e = 0.0005$ s is the electromagnetic time constant and p is the Laplace operator.

In order to keep the conducted tests objective, a constant set of RBFNN parameters is assumed. It consists of neuron's centers vector $\boldsymbol{C}$ and neural network's initial weight coefficients vector $\boldsymbol{w}$. The actual neuron's centers and initial weights values are presented below:

- $c_1 = -1$,
- $c_2 = -0.5$,
- $c_3 = 0$,
- $c_4 = 0.5$,
- $c_5 = 1$,
- $w_1 = -0.1308$,
- $w_2 = -0.0434$,
- $w_3 = 0.0343$,
- $w_4 = 0.3578$,
- $w_5 = 0.2769$.

Moreover, the neural network learning rate coefficient and Gauss scaling factor take consecutive values:

- $\eta = 0.5$,
- $\sigma = 0.5$.

In order to obtain unfavorable test conditions and to force frequent speed returns of the drive, a square wave was chosen as a speed reference signal. It features consecutive parameters:

- $Amp = 0.25$,
- $f = 0.15$ Hz.

The speed controller deployed in the examined structure is based on the speed error. Electric motors are characterized by inertia, which limits their dynamic capabilities. Thus, in order not to force the motor to follow the trajectory which in fact cannot be reached and to avoid unnecessary stimulation of the control structure during the dynamics states, the reference signal is passed through a filter.

A thorough analysis of the proposed algorithm requires the examination of various, inconvenient disturbances, attached to the drive system. Thus, an additional active load torque is attached during the simulation. The load torque attachment occurs at $t = 11.5$ s while the detachment takes place at $t = 13.5$ s. The active load torque value equals the motor nominal torque. What is more, to simulate a real electric drive unit, a control signal constraint is applied to prevent power converter damage. It equals $\pm 3T_{en}$. Furthermore, in order to examine the control system behavior when the plant parameters are changed, the set of tested load time constant variants consists of three values:

- $T_2 = T_{2n}$,
- $T_2 = 3T_{2n}$,
- $T_2 = 5T_{2n}$.

The first attempt involves the comparison of the default ADRC approach with the proposed control solution. The value of the load machine time constant is nominal. The obtained speed transients and zoom-in figures, showing the system response after additional load torque attachment, are shown in Figs. 5(a) and 5(b).

Speed transients obtained during the first simulation test stage (Figs. 5 and 6) demonstrate the correctness of the drive response in both cases. The system behavior is eligible. The actual load machine speed value follows the reference trajectory correctly. However, the zoom-in presented in Fig. 6 emphasizes the positive impact of the neural adjuster. The overshoot visible after additional

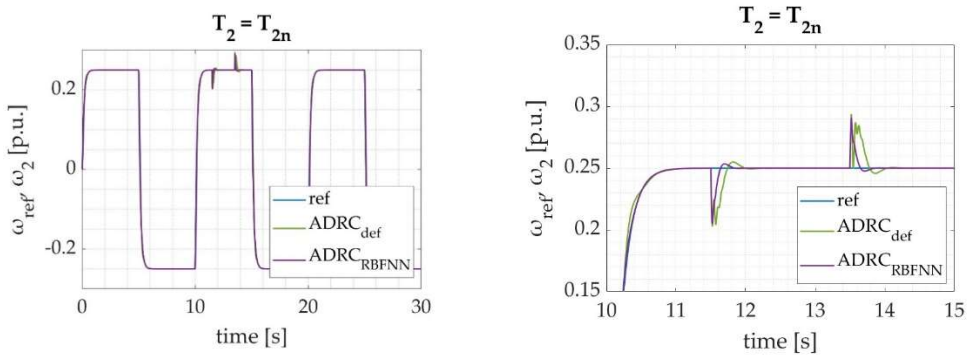

Fig. 5. Speed transients for default plant parameters (a); a zoom-in showing a moment of additional load torque attachment, detachment, and a steady-state transition (b)

load torque attachment is smaller for the RBFNN supported strategy. What is more, the plant response in the proposed solution is slightly better in the dynamic states of the drive than in the default control system. Speed is brought back to the steady state quicker, and is visibly less rugged. Additionally, the actual speed value follows the reference trajectory more accurately.

The next stage of the simulation tests involves the increased load machine time constant ($T_2 = 3T_{2n}$). The results are presented in Figs. 6(a) and 6(b).

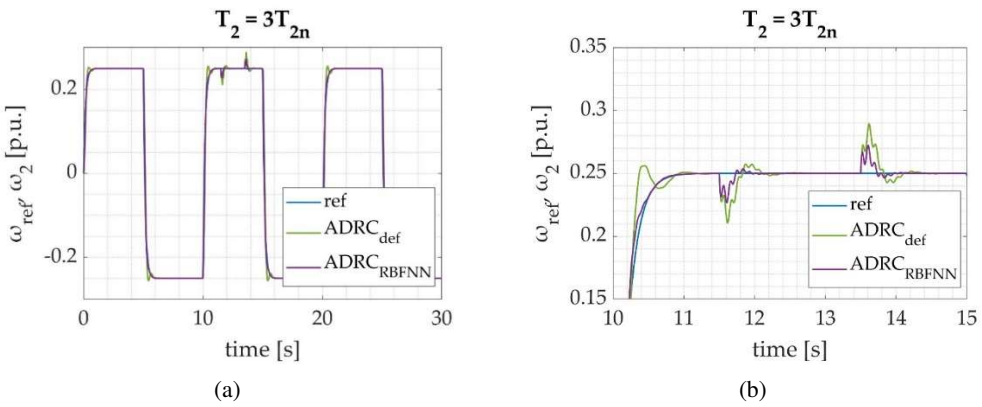

Fig. 6. Speed transients obtained for a changed mechanical time constant of the plant ($T_2 = 3T_{2n}$) (a); a zoom-in showing a moment of additional load torque attachment, detachment, and a steady-state transition (b)

Speed transients obtained during the second stage of numerical tests present a visible difference in control systems behavior. There is a significant lurch, which occurs during the steady-state transition in the default ADRC control strategy. The comparison of the two examined control algorithms proves that the RBFNN equipped control system mitigates the occurred lurch and makes the system follow the reference speed more accurately. Moreover, the overshoots occurring

during additional load torque attachment and detachment is smaller as well. The proposed ADRC adjustment extension lowers the susceptibility to the changed plant parameters, which makes the whole ADRC strategy more versatile.

The third part of the numerical examination involved extremely increased mechanical time constant, which equaled $T_2 = 5T_{2n}$ The obtained results are presented in Figs. 7(a) and 7(b).

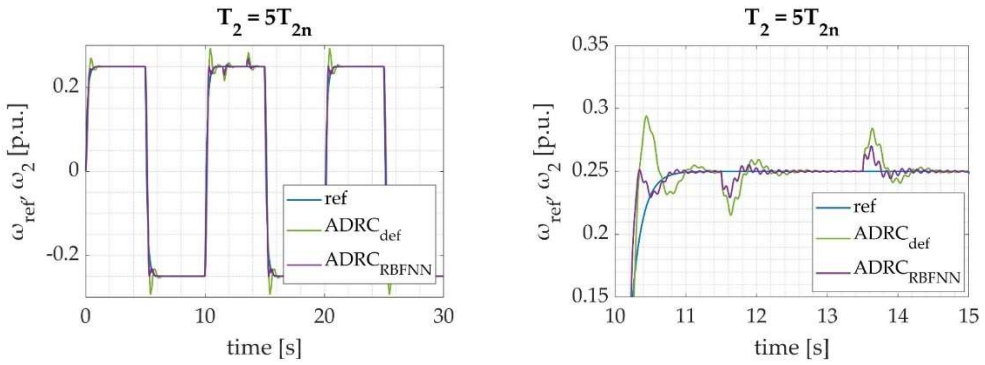

(a) (b)

Fig. 7. Speed transients obtained for a changed mechanical time constant of the plant ($T_2 = 5T_2$) (a); a zoom-in showing a moment of additional load torque attachment, detachment, and a steady-state transition (b)

The last attempt of the conducted simulations proves that the applied ADRC neural adjuster improves the overall system performance. Both algorithms handle the speed control issue eligibly when the mechanical time constant of the load machine is extremely increased. However, the speed lurch occurring in the proposed solution is significantly lower than the one in the standard ADRC approach. Moreover, the overshoot is mitigated in the developed algorithm. The visible difference is a crucial improvement regarding the enormous plant parameter change. The system response to the additional load torque attachment and detachment is better as well.

In order to emphasize the positive neural network response in each case, Fig. 8 includes the RBFNN output transients depending on the plant parameters.

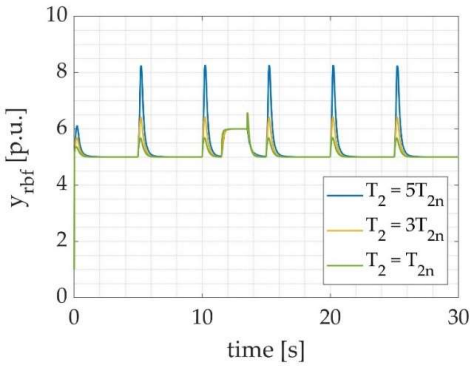

Fig. 8. RBFNN output transients depending upon the load machine mechanical time constant value

5. Experimental tests

The second stage of the tests includes the experimental deployment of the algorithm. The whole control structure is implemented on the laboratory stand. The main part of the test-bench consists of two 0.5 kW D.C. motors coupled together with a long, resilient shaft. The role of the shaft is to introduce additional elasticity to the mechanical part of the drive. What is more, additional flywheel weight is attached to the load machine shaft to simulate a hypothetical mechanical time constant change. Each electric motor is powered with its independent four-quadrant H-bridge power converter. The role of the load machine is also fulfilled by an electric motor, as the presented solution allows active load torque attachment, which improves the objectivity of the conducted experiments. Each electric motor is also attached to the rotary encoder featuring 36 000 pulses per revolution. The whole laboratory setup is powered with an autotransformer. The control structure is deployed on the dSPACE 1103 rapid-prototyping system equipped with a digital signal processor. In order to obtain relevant torque control, a typical cascade structure is implemented. The current measurement was accomplished with an LEM transducer. The whole experimental process is controlled with the use of a master PC, equipped with ControlDesk software. The proposed test bench ensures high computational power combined with versatile, real-time control capabilities. The overall scheme of the laboratory stand is presented in Fig. 9. The actual photos of particular test-bench components are presented in Fig. 10.

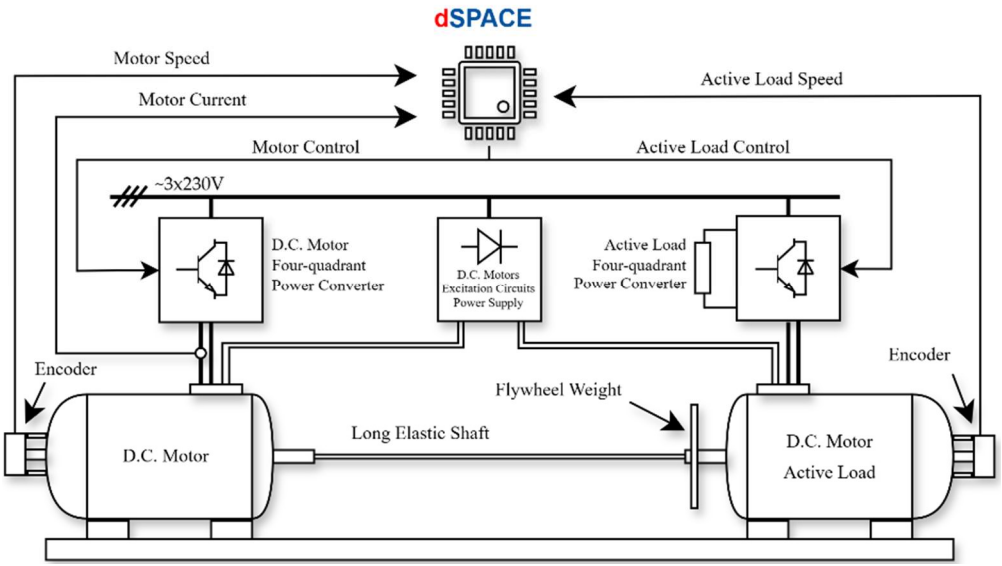

Fig. 9. The overall scheme of the laboratory stand used during experimental verification of the proposed algorithm

The most important parameters of the presented test-bench are collected below:

- Nominal motor power: 500 W,
- Nominal rotational speed: 1450 rpm,
- DC motor mechanical time constant: 0.203 s,

– DC load machine mechanical time constant: 0.208 s,
– Elastic shaft mechanical time constant: 0.0026 s,
– Nominal encoder resolution: 36 000 p./rev.

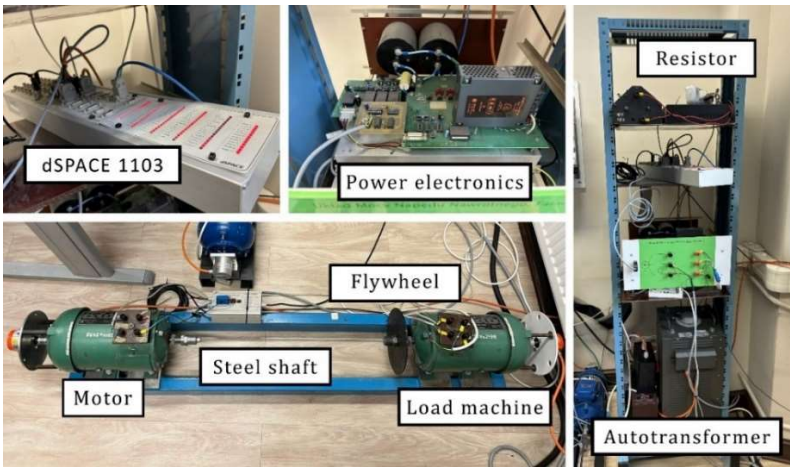

Fig. 10. Particular components of the laboratory setup

The experimental verification of the proposed algorithm involves the comparison of the control system response regarding the default and increased mechanical time constant of the plant. In the first stage of the conducted tests the standard ADRC algorithm behavior is examined. For the sake of the experimental deployment, a square wave is chosen as a reference signal. The parameters of the reference speed trajectory are presented below:

– $Amp = 0.4$,
– $f = 0.1$ Hz.

During every second speed return additional active load torque is attached to the system. The first attempt concerns the default and increased ($T_2 = 3T_{2n}$) plant parameters. The obtained results are presented in Figs. 11(a) and 11(b).

Speed transients obtained during the experimental tests show the differences between the plant response when the plant parameters are changed. Despite the fact that the overall system behavior can be considered eligible in both cases, a visible lurch occurred in the second attempt (increased load machine inertia). Thus, in order to mitigate the speed transient during the steady-state transition, controller gains can be increased. However, passive enhancement of the coefficients may lead to serious problems, which occurred during the second part of the tests (Fig. 12). The speed transient demonstrates an inconvenience which occurred for the structure with passively increased controller gains. The lurch visible in the previous attempt was mitigated. However, it turned out that the system response became oscillatory after additional active load torque detachment and could not be damped. Thus, the obtained results emphasize the prevalence of the proposed solution over a standard ADRC approach, as the active, floating coefficient adjusts controller gains on the fly and increases the robustness of the system effectively.

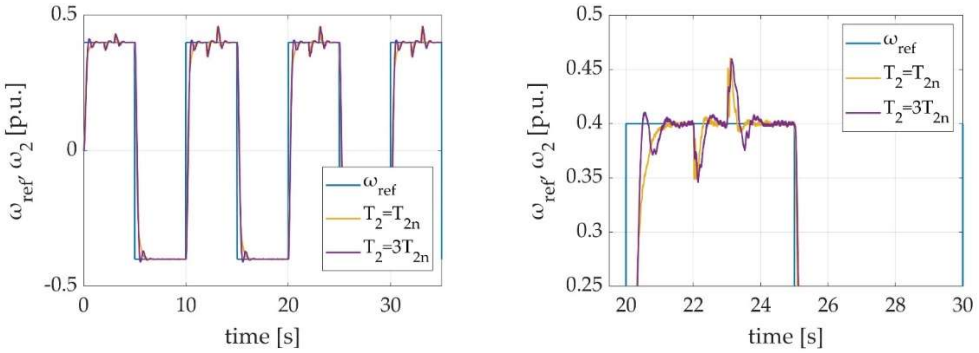

(a) (b)

Fig. 11. Speed transients for experimental tests of the standard ADRC algorithm and both default and increased ($T_2 = 3T_{2n}$) mechanical time constant of the load machine (a); a zoom-in showing a steady-state transition and system response on the additional load torque attachment and detachment (b)

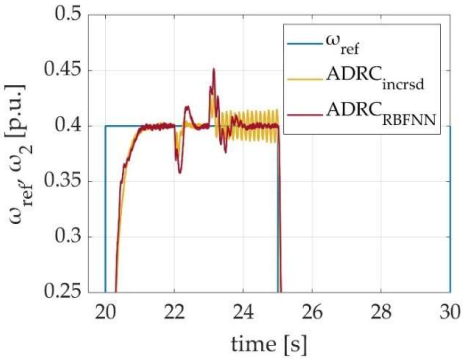

Fig. 12. Speed transients obtained during experimental tests for the modified ADRC algorithms and increased ($T_2 = 3T_{2n}$) mechanical time constant of the load machine: a zoom-in showing a steady-state transition and system response on the additional load torque attachment and detachment. $\text{ADRC}_{\text{incrsd}}$– controller gains increased with a constant value, $\text{ADRC}_{\text{RBFNN}}$ – Neural Network based ADRC adjuster

6. Conclusions

The presented approach demonstrates an extended ADRC load-side speed controller. The contribution of the paper lies in the improvement of the classic approach through the addition of an RBFNN. The neural network adjusts the controller parameters in a limited range, according to the demanded system dynamics. Because of this, the robustness of the control structure is further improved. The following advantages are achieved:

– ADRC in its standard form provides satisfactory results, even when the load inertia is increased 3 times. The only issue is small overshoots and lurches visible during steady-state transitions.

– The controller gains are adjusted during the operation of the drive, guaranteeing smooth transitions between steady states. At the same time, speed oscillations after load torque deactivation are successfully mitigated.
– The control structure operates solely based on information about the speed of the load machine (the information about the speed of the motor is not necessary). Because of that, the reliability of the drive is increased.
– Because of a smaller number of sensors in the control structure, its overall cost is effectively reduced.
– The use of the proposed algorithm significantly improves the overall plant response and drive system quality without the necessity of plant parameters adjustment (b coefficient).

Further improvements of the control algorithm can be sought in optimization of the neural network parameters. The training starting point, as well as the range in which the controller gains are adjusted could be obtained through the use of a genetic (or other nature-inspired) algorithm. Nevertheless, the obtained results are very promising and constitute a great basis for industrial motor control applications.

References

[1] Wang H., Zhang Q., Feng Y., Chen I.M., *Robust Terminal Sliding Mode Tracking Control for Flexible-Joint Robots*, The Proceedings of 46th Annual Conference of the IEEE Industrial Electronics Society, Singapore, pp. 5094–5098 (202), DOI: 10.1109/IECON43393.2020.9254927.

[2] Yang H., Wei P., Zhang Y., Liu X., Yang L., *Disturbance Observer Based on Biologically Inspired Integral Sliding Mode Control for Trajectory Tracking of Mobile Robots*, IEEE Access, vol. 7, pp. 48382–48391 (2019), DOI: 10.1109/ACCESS.2019.2907126.

[3] Yin Y., Liao M., Lyu P., *The dynamic stability analysis of wind turbines under different control strategies*, The Proceedings of 5th International Conference on Electric Utility Deregulation and Restructuring and Power Technologies (DRPT), pp. 2581–2586 (2015), DOI: 10.1109/DRPT.2015.7432683.

[4] Ristiana R., Hindersah H., Rohman A.S., Machbub C., Purwadi A., Rijanto E., *Torque control using integrated battery-electric vehicle model with flexible shaft*, The Proceedings of 4th International Conference on Electric Vehicular Technology (ICEVT), Bali, Indonesia, pp. 24–29 (2017), DOI: 10.1109/ICEVT.2017.8323528.

[5] Salehian M., Sattarzadeh S., Talebi H.A., Bayat M., Asehabi A., *Vibration suppression of a flexible shaft system using indirect adaptive control*, The Proceedings of 3rd International Conference on Control, Instrumentation, and Automation, Tehran, Iran, pp. 301–306 (2013), DOI: 10.1109/ICCIAutom.2013.6912853.

[6] Pourebrahim M., Ayati M., Mahjoob M., *Design and implementation of PI and fuzzy PID supervisory controllers for a flexible link robot*, The Proceedings of 2nd International Conference on Control Science and Systems Engineering (ICCSSE), Singapore, pp. 270–275 (2016), DOI: 10.1109/CCSSE.2016.7784396.

[7] Szabat K., Orlowska-Kowalska T., *Vibration Suppression in a Two-Mass Drive System Using PI Speed Controller and Additional Feedbacks—Comparative Study*, IEEE Transactions on Industrial Electronics, vol. 54, no. 2, pp. 1193–1206 (2007), DOI: 10.1109/TIE.2007.892608.

[8] Trung T.V., Furuta T., Akita K., Iwasaki M., *Full State Feedback-based Vibration Suppression Control of Flexible- Link Flexible-Joint Robot*, The Proceedings of IEEE 30th International Symposium on Industrial Electronics (ISIE), Kyoto, Japan, pp. 1–6 (2021), DOI: 10.1109/ISIE45552.2021.9576460.

[9] Tarczewski T., Szczepanski R., Erwinski K., Hu X., Grzesiak L.M., *A Novel Sensitivity Analysis to Moment of Inertia and Load Variations for PMSM Drives*, IEEE Transactions on Power Electronics, vol. 37, no. 11, pp. 13299–13309 (2022), DOI: 10.1109/TPEL.2022.3188404.

[10] Shikata K., Katsura S., *Hierarchical Control for Vibration Suppression Through Decoupling of Traveling/Reflected Waves*, The Proceedings of 49th Annual Conference of the IEEE Industrial Electronics Society, Singapore, Singapore, pp. 1–6 (2023), DOI: 10.1109/IECON51785.2023.10312496.

[11] Vinida K., Chacko M., *A novel strategy using H infinity theory with optimum weight selection for the robust control of sensorless brushless DC motor*, The Proceedings of IEEE Symposium on Sensorless Control for Electrical Drives (SLED), Nadi, Fiji, pp. 1–5 (2016), DOI: 10.1109/SLED.2016.7518799.

[12] Derugo P., *Transfer learning for fuzzy control of two-mass drive system using state variables feedback*, The Proceedings of 10th International Conference on Electrical, Electronic and Computing Engineering (IcETRAN), East Sarajevo, Bosnia and Herzegovina, pp. 1–6 (2023), DOI: 10.1109/IcETRAN59631.2023.10192221.

[13] Wu A.G., Dong R.Q., Zhang Y., He L., *Attitude stabilization for flexible spacecraft with inertia uncertainty by a sliding mode control law*, The Proceedings of 12th Asian Control Conference (ASCC), Kitakyushu, Japan, pp. 1472−1477 (2019).

[14] Han J., *From PID to Active Disturbance Rejection Control*, IEEE Transactions on Industrial Electronics, vol. 56, no. 3, pp. 900–906 (2009), DOI: 10.1109/TIE.2008.2011621.

[15] Qu K., Cheng C., Hua W., *Speed fluctuation Suppression of PMSM Based on Repetitive Active Disturbance Rejection Control*, The Proceedings of 26th International Conference on Electrical Machines and Systems (ICEMS), Zhuhai, China, pp. 1073–1077 (2023), DOI: 10.1109/ICEMS59686.2023.10345305.

[16] Lv X., Zhu J., Qiao T., Song X., *Study of PMSM Servo System Based on A Novel Fuzzy Active Disturbance Rejection Controller*, The Proceedings of 6th International Conference on Automation, Control and Robotics Engineering (CACRE), Dalian, China, pp. 140–144 (2021), DOI: 10.1109/CACRE52464.2021.9501388.

[17] Du Y., Cao W., She J., Fang M., *A Comparison Study of Three Active Disturbance Rejection Methods*, The Proceedings of 39th Chinese Control Conference (CCC), Shenyang, China, pp. 135−139 (2020), DOI: 10.23919/CCC50068.2020.9189230.

[18] Kabziński J., *Adaptive friction compensation in two-mass drive system with flexible shaft*, Proceedings of 2nd International Conference on Measurement, Information and Control, Harbin, China, pp. 874–878 (2013), DOI: 10.1109/MIC.2013.6758100.

[19] Zhong C., Guo Y., Yu Z., *A self-adjusting sliding-mode control based on RBF neural network for flexible spacecraft attitude*, Proceedings of IEEE International Conference on Information and Automation (ICIA), Yinchuan, China, pp. 207–212 (2013), DOI: 10.1109/ICInfA.2013.6720297.

[20] Wu X., Wang C., Xu C., Liu K., Wang G., Sun Z., *An Adaptive Control Method Based on Radial Basis Function Neural Network for Variable Stiffness Actuator*, Proceedings of IEEE International Conference on Industrial Technology (ICIT), Bristol, United Kingdom, pp. 1–6 (2024), DOI: 10.1109/ICIT58233.2024.10540877.

[21] Wicher B., Brock S., *Active disturbance rejection control based load side speed controller for two mass system with backlash*, Proceedings of IEEE 18th International Power Electronics and Motion Control Conference (PEMC), pp. 645–650 (2018), DOI: 10.1109/EPEPEMC.2018.8522001.

[22] Wicher B., *ADRC load position controller for two mass system with elastic joint and backlash*, Proceedings of 23rd International Conference on Methods & Models in Automation & Robotics (MMAR), pp. 333–338 (2018), DOI: 10.1109/MMAR.2018.8486007.

[23] Norris G., Ducard G.J.J., Onder C., *Neural networks for control: A tutorial and survey of stability-analysis methods, properties, and discussions*, Proceedings of International Conference on Electrical, Computer, Communications and Mechatronics Engineering (ICECCME), pp. 1–6 (2021), DOI: 10.1109/ICECCME52200.2021.9590912.

[24] Fadali M.S., *On the stability of han's adrc*, Proceedings of American Control Conference, pp. 3597–3601 (2014), DOI: 10.1109/ACC.2014.6859248.